CANCER BIOTHERAPY AND RADIOPHARMACEUTICALS
Volume 30, Number 1, 2015

DOI: 10.1089/cbr.2014.1709

Spatial Resolution and Image Qualities of Zr-89 on Siemens Biograph TruePoint PET/CT

Young Sub Lee,[1,2] Jin Su Kim,[1] Jung Young Kim,[1] Byung Il Kim,[1] Sang Moo Lim,[1] and Hee-Joung Kim[2]

Abstract

Purpose: Zirconium-89 ($t_{1/2}$ = 78.41 hours) is an ideal metallic radioisotope for immuno–positron emission tomography (PET), given that its physical half-life closely matches the biological half-life of monoclonal antibodies. In this study, the authors measured the spatial resolution and image quality of Zr-89 PET and compared the results against those obtained using F-18 PET, which is widely regarded as the gold standard for comparison of imaging characteristics.
Materials and Methods: The spatial resolution and image qualities of Zr-89 were measured on the Siemens Biograph Truepoint TrueV PET/CT scanner, partly according to NEMA NU2-2007 standards. For spatial resolution measurement, the Zr-89 point source was located at the center of the axial field of view (FOV) and offset 1/4 axial FOV from the center. For image quality measurements, an NEMA IEC Phantom was used. The NEMA IEC Phantom consists of six hot spheres that were filled with Zr-89 solution. Spatial resolution and image quality (%contrast, %background variability [BV], and source to background ratio [SBR]) were assessed to compare the imaging characteristics of F-18 with those of Siemens Biograph Truepoint TrueV.
Results: The transverse and axial spatial resolutions at 1 cm were 4.5 and 4.7 mm for Zr-89, respectively. The %contrast of Zr-89 was 25.5% for the smallest 10 mm sized sphere and 89.8% for the largest 37 mm sized sphere, and for F-18, it was 32.5% for the smallest 10 mm sized sphere and 103.9% for the largest 37 mm sized sphere using the ordered subset expectation maximization (OSEM) reconstruction method. The %BV of F-18 PET was 6.4% for the smallest 10 mm sized sphere and 3.5% for the largest 37 mm sized sphere using the OSEM reconstruction. The SBR of Zr-89 was 1.8 for the smallest 10 mm sized sphere and 3.7 for the largest 37 mm sized sphere, and for F-18, it was 2.0 for the smallest 10 mm sized sphere and 4.1 for the largest 37 mm sized sphere using the OSEM reconstruction method.
Conclusions: This study assessed Zr-89 imaging characteristics using a Siemens Biograph Truepoint TrueV PET/CT scanner and compared the results with those obtained for F-18 PET. Although spatial resolution and image quality of Zr-89 PET were lower compared with F-18 PET, due to longer positron range and low positron branching ratio, Zr-89 is advantageous for immuno-PET due to well-matched half-life with monoclonal antibodies.

Key words: Zr-89, image quality, PET, radioimmunotherapy (RIT), spatial resolution

Introduction

Radioimmunotherapy (RIT) is a promising approach for targeted therapy to treat intractable cancer because radionuclides are selectively delivered to a tumor using monoclonal antibodies.[1] In RIT, an accurate calculation of the absorbed dose is important for accurate and reproducible patient treatment. Generally, radiation absorbed dose estimates use whole-body gamma camera planar imaging or single-photon emission computed tomography (SPECT) imaging.[2,3] Various correction methods have been established to improve the accuracy of the absorbed dose in gamma camera planar or SPECT imaging for RIT.[4–6] However, gamma camera or SPECT imaging has some limitations, including poor spatial resolution and image quality. Positron emission tomography (PET) systems are generally more sensitive than both SPECT and gamma camera systems, and have better spatial resolution and image quality.[7] PET is

[1]Molecular Imaging Research Center, Korea Institute of Radiological and Medical Sciences, Seoul, Republic of Korea.
[2]Department of Radiation Convergence Engineering, Research Institute of Health Science, Yonsei University, Wonju, Republic of Korea.

Address correspondence to: Jin Su Kim; Molecular Imaging Research Center, Korea Institute of Radiological and Medical Sciences; 75 Nowon-gil, Gongneung-Dong, Nowon-Gu, Seoul 139-706, Republic of Korea
E-mail: **kjs@kirams.re.kr**

Table 1. The Physical Characteristics of Zr-89, I-124, and F-18

Properties	*Zr-89*	*I-124*	*F-18*
Half-life	78.4 hour	4.18 day	109.8 min
Mean $\beta+$ energy	0.40 MeV	0.83 MeV	0.25 MeV
Mean $\beta+$ range in water	1.23 mm	3.48 mm	0.62 mm
Single γ energy	909 keV (99.9%) 1657 keV (0.1%) 1713 keV (0.8%)	602 keV (61%) 723 keV (10%) 1691 keV (11%)	
Positron branching ratio	23%	23%	97%

widely used in the nuclear medicine field. In particular, PET imaging can allow assessments of receptor occupancy or follow-up assessments for RIT (known as immuno-PET).

Immuno-PET is particularly useful for the prediction of cancer treatment with monoclonal antibodies (mAbs)[8,9] labeled with I-124 or Zr-89, because I-124 ($t_{1/2}=4.18$ d, $\beta^+=0.40$ MeV) or Zr-89 ($t_{1/2}=78.41$ hours, $\beta^+=0.83$ MeV) is an ideal radioisotope for immuno-PET because its physical half-life is similar to the biological half-life of mAbs.[8] Table 1 summarizes physical characteristics of Zr-89, I-124, and F-18. A longer positron range and a poor positron branching ratio of Zr-89 or I-124 may result in poor image quality.[10] To the best of knowledge, there was no report for resolution and image quality characteristics of Zr-89 in the clinical PET scanner using various reconstruction methods. In this study, the authors measured the spatial resolution and image quality of Zr-89 PET and compared the results to those obtained for F-18 PET, the current gold standard for comparison of imaging characteristics.

Materials and Methods

To compare the imaging characteristics between Zr-89 and F-18 PET, spatial resolution and image quality were measured on a Siemens Biograph Truepoint TrueV PET/CT scanner, partly according to NEMA NU2-2007 standards.[11,12] The radioisotope F-18 was prepared by nuclear reaction as O-18(p, n)F-18 in liquid target for F-18 at medical cyclotron (MC-50, Scantronix Co., 1985), while the radioisotope Zr-89 was produced by a nuclear reaction as Y-89(p, n)Zr-89 in solid target at the above same cyclotron. To obtain high radiochemical purity, Zr-89 was used as the chemical form of zirconium oxalate purified by a specific resin column method as reference.[13] For the quality control of the Zr-89 isolated from column, the radionuclidic purity of >99.9% was found to be analyzed by gamma-ray spectroscopy (HPGe detector; Ortec Co.), confirming the inherent energy of 511 and 909 KeV with the absence of other radionuclidic impurities. The radiochemical purity was also shown to be >99.9% by instant thin-layer chromatography (ITLC paper) and the radio-TLC scanner (AR-2000; Eckert & Ziegler Co.).

System description and data acquisition

The Siemens Biograph Truepoint TrueV PET/CT scanner is designed for high-resolution imaging with increased sensitivity using an extended field of view (FOV) and improved spatial resolution using PSF modeling reconstruction (TrueX).[12,14] Table 2 summarizes its specification. PET data were reconstructed using filtered back projection (FBP), ordered subset expectation maximization (OSEM) (iteration: 4, subset: 16), or TrueX reconstruction (TrueX) (iteration 8, subset: 21) in this study. The all-pass filter was used for OSEM and TrueX reconstruction. PET data were acquired in an energy window of 425–650 keV. The image matrix size was $336\times336\times148$ with pixel sizes of $0.51\times0.51\times1.50\,mm^3$.

Spatial resolution

For spatial resolution measurements, a point source (diameter: 1.1 mm) was made. Total activity was 3.7 MBq for the acquisition. The Zr-89 point source was located at the center of the axial FOV and offset 1/4 axial FOV from the center. The point source was positioned at three locations in the transaxial plane as follows: $x=0$ cm, $y=1$ cm; $x=0$ cm, $y=10$ cm; and $x=10$ cm, $y=0$ cm. At each position, at least 100,000 counts were acquired to enable accurate statistical analysis. For reconstruction, FBP with a ramp filter was used according to NEMA NU2-2007 standards.[11] The spatial resolution was calculated for each point source position as full width at half maximum (FWHM) and full width at tenth maximum (FWTM) of the point spread function determined in all three directions. Radial and tangential resolutions for each radial position (1 and 10 cm) were averaged for both of the axial positions according to NEMA NU2-2007 standards.[11] The spatial resolution obtained with Zr-89 PET was compared with that obtained using F-18 PET.[14]

Image quality

To compare the imaging quality between Zr-89 and F-18 PET, the NEMA international electrotechnical commission (IEC)

Table 2. Specification of Siemens Biograph TruePoint TrueV Scanner

Characteristics	*Value*
Detector material	Lutetium oxyorthosilicate (LSO)
Crystal dimensions (mm)	$4\times4\times20$
Detector elements per block	169
Plan spacing (mm)	2
Number of detector rings	52
Number of detector blocks	192
Axial FOV (mm)	216
Transaxial FOV (mm)	605
Number of contiguous image planes	109
Coincidence time window (ns)	4.5
Energy Window (keV)	425–650

FOV, field of view.

Phantom was used.[11] The NEMA IEC phantom consists of six hot spheres (ID, 10, 13, 17, 22, 28, and 37 mm) that were filled with Zr-89 solution. PET data acquired for 10 minutes. The activity concentration in the background was 5.3 kBq/cc and the activity concentration of Zr-89 in the spheres was four times the background activity. Image qualities such as percent contrast, background variability, and source to background ratio (SBR) were assessed to compare imaging characteristics of F-18.

Percent contrast (%contrast)

To calculate the contrast, transverse images obtained from the NEMA IEC Phantom were used for analysis. Regions of interest (ROIs) were drawn on each sphere. The size of ROIs was equal to the inner diameter of the sphere. The ROIs were drawn on ±2 slices from the center slice. Twelve ROIs were drawn on each slice in the background, with a total of 60 ROIs on the five slices analyzed. The %contrast $Q_{H,j}$ for sphere j was calculated as follows:

$$Q_{H,j} = \frac{C_{H,j}/C_{B,j} - 1}{a_H/a_B - 1} \times 100\%$$

Where $C_{H,j}$ is the average count in the ROI for sphere j, $C_{B,j}$ is the average of the background ROI counts for the sphere, a_H is the activity concentration in the spheres, and a_B is the activity concentration in the background.

Percent background variability (%BV)

The percent background variability N_j for sphere j was calculated as follows:

$$N_j = SD_J/C_{B,J} \times 100\%$$

Where SD_J is the standard deviation of the background ROI counts for sphere j. SD_J was calculated as follows:

$$SD_J = \sqrt{\sum_{K=1}^{K} (C_{B,J,K} - C_{B,J})^2/(K-1)},$$

where $K = 60$.

TABLE 3. THE SPATIAL RESOLUTION (FWHM/FWTM IN MM) OF ZR-89 FOR FBP, OSEM, AND TRUEX RECONSTRUCTION METHOD

	FBP	*OSEM*[a]	*TrueX*[b]
1 cm radius			
Transverse (mm)	4.5/8.2[‡]	4.3/7.9	2.5/4.5
Axial (mm)	4.7/8.5	4.3/7.9	3.3/6.0
10 cm radius			
Transverse tangential (mm)	4.6/8.4	4.9/8.0	2.5/4.6
Transverse radial (mm)	4.9/8.9	4.4/7.9	2.5/4.6
Axial (mm)	4.9/9.0	4.9/8.9	2.5/4.6

Matrix size: $336 \times 336\,mm^2$, zoom factor: 4.0, pixel size: $0.51 \times 0.51\,mm^2$.

[a]OSEM (Iteration: 4, Subset: 16 with all-pass filter).

[b]TrueX (Iteration: 8, Subset: 21 with all-pass filter).

FWHM, full width at half maximum; FWTM, full width at tenth maximum; FBP, filtered back projection; OSEM, ordered subset expectation maximization.

Source to background ratio

SBR was calculated using the same ROI that was used in the analysis of %contrast. The SBR was calculated as follows:

$$SBR = C_J/C_{B,J} \times 100\%$$

Jaszczak Phantom image

PET data of Zr-89 and F-18 using Jaszczak phantom were also acquired. Acquisition time was 10 minutes. The Jaszczak phantom consists of six sets of cold rod (ID: 4.8, 6.4, 7.9, 9.5, 11.1, and 12.7 mm). The activity in the Jaszczak phantom was 74 MBq for Zr-89 and F-18 solution. The activity concentration was 10.9 kBq/cc. Data were reconstructed using FBP, OSEM, or TrueX.

Results

Spatial resolution

The spatial resolutions for Zr-89 reconstructed using FBP, OSEM, or TrueX are tabulated in Table 3. The transverse and axial spatial resolution at 1 cm for Zr-89 was 4.5 mm FWHM and 4.7 mm FWHM in the present study and for F-18 was 4.10 mm FWHM and 4.7 mm FWHM according to the result by Jaokoby et al.[14]

Image quality

Table 4 and Figure 1A–C show the corresponding results of %contrast, %BV, and SBR for both Zr-89 and F-18 PET. Figure 2 shows transaxial images of the NEMA IEC

TABLE 4. COMPARISON OF IMAGE QUALITY (%CONTRAST, %BV, AND SBR) BETWEEN ZR-89 AND F-18

Sphere size (mm)	*Zr-89*			*F-18*		
	FBP	*OSEM*[a]	*TrueX*[b]	*FBP*	*OSEM*[a]	*TrueX*[b]
Percent contrast (%contrast)						
37	83.4	89.8	98.0	101.8	103.9	112.8
28	72.5	79.6	87.6	93.6	95.2	108.9
22	68.7	76.4	84.1	82.8	81.0	94.7
17	50.9	62.0	79.6	62.3	70.4	90.1
13	31.9	43.2	56.3	41.9	48.4	77.3
10	19.1	25.5	50.8	24.5	32.5	56.2
Percent background (%BV)						
37	6.6	4.1	6.6	7.4	3.5	4.6
28	7.5	4.9	7.1	7.9	3.6	5.6
22	7.5	5.9	8.2	8.1	3.8	5.3
17	9.1	7.7	11.0	8.3	5.0	6.2
13	13.0	10.1	14.9	8.9	5.5	7.2
10	17.3	12.3	18.7	9.7	6.4	8.2
Source to background ratio (SBR)						
37	3.5	3.7	3.9	4.1	4.1	4.4
28	3.2	3.4	3.6	3.8	3.9	4.3
22	3.1	3.3	3.5	3.5	3.5	3.8
17	2.5	2.9	3.4	2.9	3.2	3.6
13	2.0	2.3	2.7	2.3	2.5	3.3
10	1.6	1.8	2.5	1.7	2.0	2.6

[a]OSEM (Iteration: 4, Subset: 16 with all-pass filter).

[b]TrueX (Iteration: 8, Subset: 21 with all-pass filter).

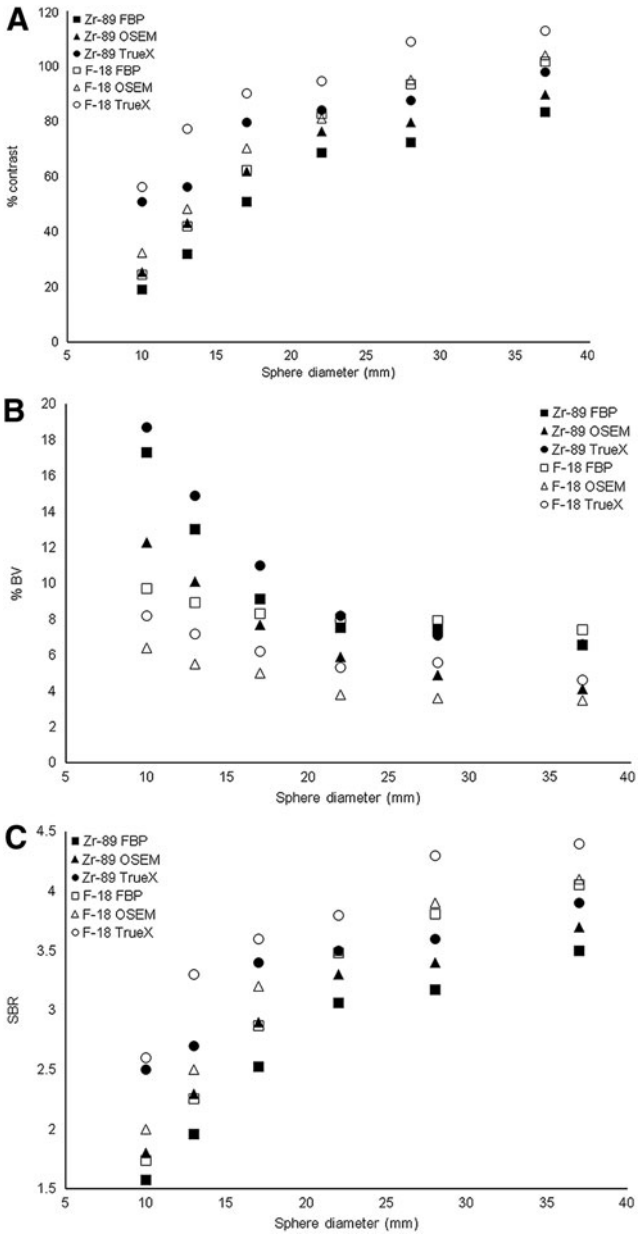

FIG. 1. Image quality results of Zr-89 and F-18. **(A)** %Contrast, **(B)** %BV, **(C)** SBR. *Closed* mark was for Zr-89 and *open* mark was for F-18. *Square* mark was for FBP, *triangle* mark was for OSEM, and *circle* mark was for TrueX. FBP, filtered back projection; OSEM, ordered subset expectation maximization; SBR, source to background ratio.

phantom with Zr-89 or F-18 using the FBP, OSEM, and TrueX reconstruction method. Quantification of %contrast, %BV, and SBR are described in the sections below.

Percent contrast (%contrast)

Table 4 and Figure 1A show the %contrast with Zr-89 and F-18 PET. The %contrast of Zr-89 PET was 19.1% for FBP, 25.5% for OSEM, and 50.8% for TrueX using the smallest 10 mm sized sphere and was 83.4% for FBP, 89.8% for OSEM, and 98.0% for TrueX using the largest 37 mm sized sphere. The %contrast of F-18 PET was 24.5% for FBP, 32.5% for OSEM, and 56.2% for TrueX using the smallest 10 mm sized sphere and was 101.8% for FBP, 103.9% for OSEM, and 112.8% for TrueX using the largest 37 mm sized sphere. When the TrueX reconstruction method was used, %contrast was highest for both Zr-89 and F-18.

Percent background variability (%BV)

The noise level, expressed as %BV, was higher for Zr-89 PET than for F-18 PET, as a result of the increase of background noise due to the poor positron branching ratio. Table 4 and Figure 1B show the %BV for Zr-89 and F-18 PET. The %BV of Zr-89 PET was 17.3% for FBP, 12.3% for OSEM, and 18.7% for TrueX using the smallest 10 mm sized sphere and was 6.6% for FBP, 4.1% for OSEM, and 6.6% for TrueX using the largest 37 mm sized sphere. The %BV of F-18 PET was 9.7% for FBP, 6.4% for OSEM, and 8.2% for TrueX using the smallest 10 mm sized sphere and was 7.4% for FBP, 3.5% for OSEM, and 4.6% for TrueX using the largest 37 mm sized sphere.

Source to background ratio

SBR represented the lesion detectability. Table 4 and Figure 1C show the SBRs for Zr-89 and F-18 PET. The SBR of Zr-89 PET was 1.6 for FBP, 1.8 for OSEM, and 2.5 for TrueX using the smallest 10 mm sized sphere and was 3.5 for FBP, 3.7 for OSEM, and 3.9 for TrueX using the largest 37 mm sized sphere. The SBR of F-18 PET was 1.7 for FBP, 2.0 for OSEM, and 2.6 for TrueX using the smallest 10 mm sized sphere and was 4.1 for FBP, 4.1 for OSEM, and 4.4 for TrueX using the largest 37 mm sized sphere. When the TrueX reconstruction method was used, SBR was the highest for both Zr-89 and F-18.

Jaszczak phantom image

Figure 3 shows transaxial images of the Jaszczak phantom with Zr-89 and F-18. The 6.4-mm-sized cold rods were well discernible for the F-18 PET image. However, the Jaszczak phantom of Zr-89 was noisy. Even 7.9-mm-sized cold rods were not clearly discernible for Zr-89 PET. This poor image quality was due to poor spatial resolution and poor %BV.

Discussion

The aim of this study was to investigate the spatial resolution and image quality characteristics of Zr-89 PET with various reconstruction methods and compared with F-18.

In this present study, the transverse spatial resolution at 1 cm for Zr-89 and F-18 was 4.5 and 4.1 mm, respectively. The transverse spatial resolution at 1 cm for Zr-89 was approximately 8.9% lower compared with F-18. According to a recent report, spatial resolution was 1.81 mm FWHM for F-18 and 1.99 mm FWHM for Zr-89 on the Inveon PET scanner.[15] The spatial resolution of Zr-89 was degraded by 10% compared to that of F-18 on the Inveon PET scanner. Theoretically, the spatial resolution corrected for source dimension for Zr-89 and F-18 on the Siemens Biograph TruePoint TrueV PET scanner can be calculated with the following equation;[10,16]

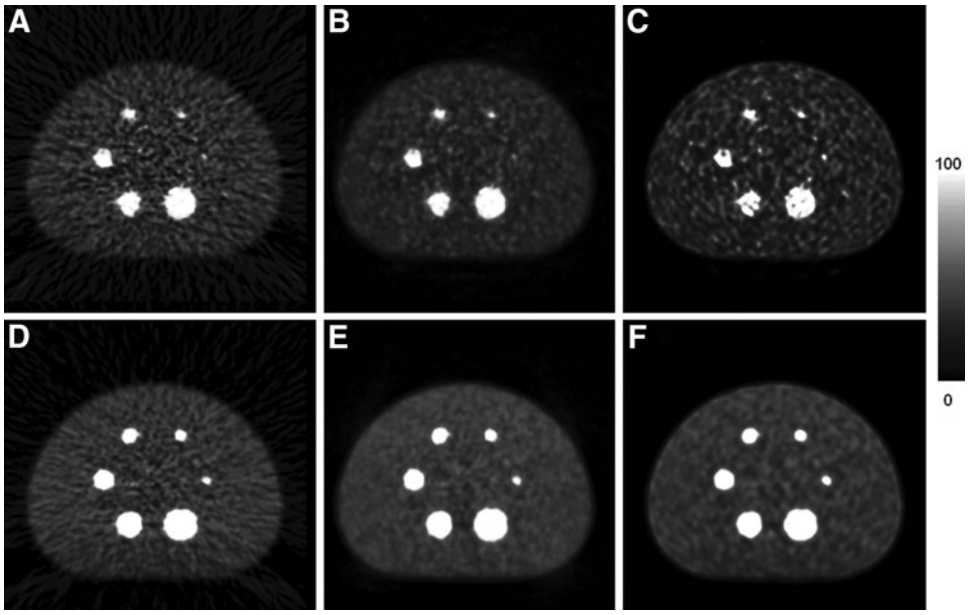

FIG. 2. Transaxial images of NEMA IEC phantom. Zr-89 images using **(A)** FBP, **(B)** OSEM, and **(C)** TrueX and F-18 images using **(D)** FBP, **(E)** OSEM, and **(F)** TrueX.

$$FWHM = 1.25\sqrt{\left(\frac{D_{crystal}}{2}\right)^2 + (0.0022D_{system})^2 + p^2 + b^2}$$

Where $D_{crystal}$ is the dimension of the crystal element and D_{system} is the ring diameter, p is the positron range (Zr-89: 1.23 mm, F-18: 0.62 mm),[15] and b is the block factor (assumed to zero). The theoretical spatial resolution values for Zr-89 and F-18 were 3.7 and 3.5 mm when the block factor was assumed to be negligible. Theoretically, spatial resolution of Zr-89 was degraded by 6.5% compared to F-18. The 909 keV gamma photon of Zr-89, as indicated, is out of the energy window (energy window: 425–650 keV), but due to its higher energy, a Compton scattering is pretty probable. Then, as the positron emission is produced in coincidence with this photon, there is a chance that the scattered photon could enter in the energy window, producing some degree of noise.

According to the previous study,[17] spatial resolution of I-124 was compared with that of F-18. Spatial resolution of I-124 was degraded by 19.9% compared to those of F-18 on the ECAT HR+ scanner. Although positron abundance of Zr-89 and I-124 was similar (Zr-89: 23% and I-124: 23%),[15] I-124 has a longer positron range (Zr-89: 1.23 mm, I-124: 3.48 mm)[15] than Zr-89, which was responsible for the poor spatial resolution of I-124 PET compared to that of Zr-89. Although the authors did not measure the spatial resolution of I-124 in this study, the theoretical value of I-124 was 5.5 mm on the Siemens Biograph TruePoint TrueV PET scanner. This was due to the longer positron range of I-124. This study showed that Zr-89 was superior to I-124 for immuno-PET in terms of resolution.

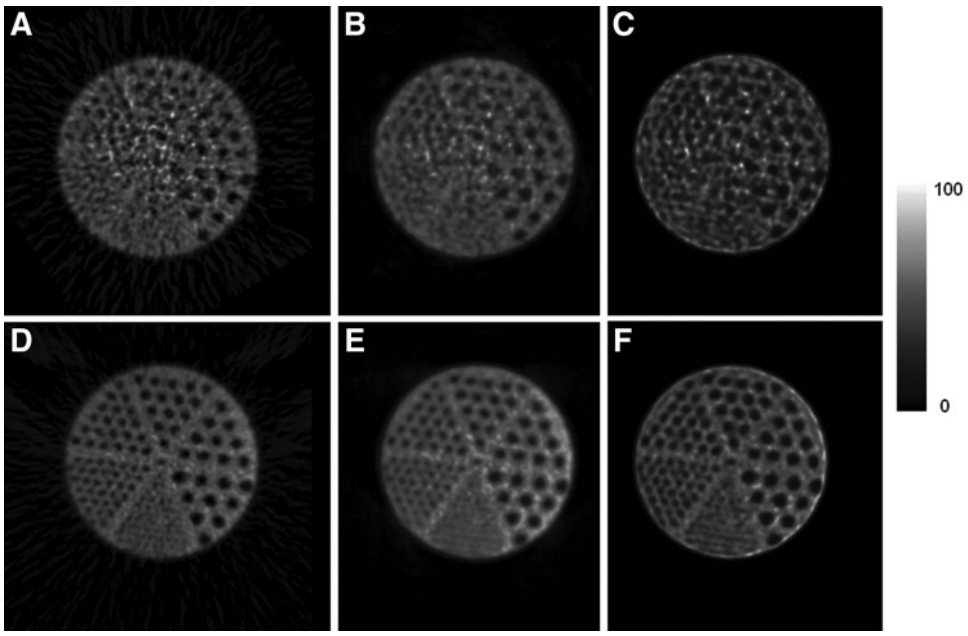

FIG. 3. Transaxial images of Jaszczak phantom. Zr-89 images using **(A)** FBP, **(B)** OSEM, and **(C)** TrueX and F-18 images using **(D)** FBP, **(E)** OSEM, and **(F)** TrueX.

The authors reported the spatial resolution and image quality for Zr-89 for the Siemens biograph true point true V scanner. Although the spatial resolution and image quality were scanner-specific values, this provided information in this study could be used for a different scanner after harmonization such as calibration of the local dose calibrator for Zr-89, postreconstruction smoothing of images, and use of VOI using the three-dimensional (3D) peak for analysis of activity according to the recent report.[8]

Although previous studies[12,14,18] compared imaging characteristics using various reconstruction algorithms such as FBP, OSEM, and PSF reconstruction, to the best of knowledge, the present study was the first report for resolution and image quality characteristics using Zr-89 with various reconstruction algorithms (FBP, OSEM, or TrueX). In this study, the authors showed that 3D PET reconstruction using a system matrix with PSF modeling provided better spatial resolution and image quality than conventional reconstruction algorithms. TrueX reconstructions exploited the spatially variant point spread function, derived from point source measurements in 3D. PSF modeling for reconstruction of image characteristics is expected to be highly improved. The SIEMENS Biograph TruePoint TrueV PET scanner provided the PSF reconstruction system (called TrueX from Siemens) with improved sensitivity due to lengthened FOV. The present study also showed that TrueX reconstruction could provide finer resolution and better %contrast compared to other conventional reconstruction algorithms such as FBP or OSEM.

Conclusions

In this study, the authors measured the spatial resolution and image quality of Zr-89 on a Siemens Biograph True point PET/CT scanner. Although spatial resolution and image quality of Zr-89 PET were lower than those of F-18 PET due to longer positron range and low positron branching ratio, Zr-89 is advantageous for immuno-PET due to well-matched half-life with monoclonal antibodies.

Acknowledgments

This work was supported by grants from the Nuclear R & D Program (2011-00300162 & 504412014) of the Korea Science and Engineering Foundation funded by the Ministry of Education, Science and Technology.

Disclosure Statement

No competing financial interests exist.

References

1. Rao AV, Akabani G, Rizzieri DA. Radioimmunotherapy for non-hodgkin's lymphoma. Clin Med Res 2005;3:157.
2. Dewaraja YK, Wilderman SJ, Koral KF, et al. Use of integrated SPECT/CT imaging for tumor dosimetry in I-131 radioimmunotherapy: A pilot patient study. Cancer Biother Radiopharm 2009;24:417.
3. Rajendran JG, Gopal AK, Fisher DR, et al. Myeloablative-I-131-tositumomab radioimmunotherapy in treating non-Hodgkin's lymphoma: Comparison of dosimetry based on whole-body retention and dose to critical organ receiving the highest dose. J Nucl Med 2008;49:837.
4. Ferrer L, Delpon G, Lisbona A, et al. Dosimetric impact of correcting count losses due to deadtime in clinical radioimmunotherapy trials involving I-131 scintigraphy. Cancer Biother Radiopharm 2003;18:117.
5. Schipper MJ, Koral KF, Avram AM, et al. Prediction of therapy tumor-absorbed dose estimates in I-131 radioimmunotherapy using tracer data via a mixed-model fit to time activity. Cancer Biother Radiopharm 2012;27:403.
6. Jonsson L, Ljungberg M, Strand SE. Evaluation of accuracy in activity calculations for the conjugate view method from Monte Carlo simulated scintillation camera images using experimental data in an anthropomorphic phantom. J Nucl Med 2005;46:1679.
7. Rahmim A, Zaidi H. PET versus SPECT: Strengths, limitations and challenges. Nucl Med Commun 2008;29:193.
8. Makris NE, Boellaard R, Visser EP, et al. Multicenter harmonization of Zr-89 PET/CT performance. J Nucl Med 2013;55:264.
9. Dongen GA, Vosjan MJ. Immuno-positron emission tomography: Shedding light on clinical antibody therapy. Cancer Biother Radiopharm 2010;25:375.
10. Tomic N, Thompson CJ, Casey ME. Investigation of the ''Block Effect'' on spatial resolution in PET detectors. IEEE Trans Nucl Sci 2005;52:599.
11. NEMA. Performance Measurements of Positron Emission Tomographs. Rosslyn, VA, NEMA Standards Publication NU 2-2007, 2007.
12. Lee YS, Kim JS, Kim KM, et al. Performance measurement of PSF modeling reconstruction (True X) on Siemens Biograph TruePoint TrueV PET/CT. Ann Nucl Med 2014; 28:340.
13. Holland JP, Sheh Y, Lewis JS. Standardized methods for the production of high specific-activity Zr-89. Nucl Med Biol 2009;36:729.
14. Jakoby BW, Bercier Y, Watson CC, et al. Performance Characteristics of a New LSO PET/CT Scanner With Extended Axial Field-of-View and PSF Reconstruction. IEEE Trans Nucl Sci 2009;56:633.
15. Disselhorst JA, Brom M, Laverman P, et al. Image-quality assessment for several positron emitters using the NEMA NU 4-2008 standards in the Siemens Inveon small-animal PET scanner. J Nucl Med 2010;51:610.
16. Kim JS, Lee JS, Im KC, et al. Performance measurement of the microPET focus 120 scanner. J Nucl Med 2007;48:1527.
17. Lee YS, Kim JS, Kim H-J, et al. Imaging Characteristics of I-124 Between 3D and 2D on Siemens ECAT HR+ PET Scanner. IEEE Trans Nucl Sci 2013;60:797.
18. Jakoby BW, Bercier Y, Conti M, et al. Physical and clinical performance of the mCT time-of-flight PET/CT scanner. Phys Med Biol 2013;56:2375.